

SPECTRAL ELEMENT METHOD PART 2: NUMERICAL SIMULATIONS

Aimé Fournier

National Center for Atmospheric
Research
Boulder CO 80307-3000 USA
fournier@ucar.edu

Lorenzo M. Polvani

Columbia University
New York NY 10027 USA
www.columbia.edu/~lmp

Mark A. Taylor

Albuquerque NM 87108 USA
www.scd.ucar.edu/css/staff/taylor

R. Saravanan

National Center for Atmospheric
Research
Boulder CO 80307-3000 USA
www.cgd.ucar.edu/gds/svn

ABSTRACT

Breaking Rossby waves on the polar night vortex are numerically simulated by solving the 3D spherical primitive equations with the *Spectral Element Atmospheric Model* described in Part 1. A balanced axisymmetric-vortex is initialized with a step-function-like absolute-vorticity profile. Steadily-increasing, zonal-wavenumber-one surface-geopotential forcing is used to instigate upwardly propagating Rossby waves. Spurious reflection is prevented by a sponge layer near the model top.

Isosurfaces of *scaled potential vorticity* exhibit complex dynamical features, e.g., a primary PV tongue, and a secondary instability causing roll-up into a ring of five smaller sub-vortices. These are shown in Figs. 3 and 4. These features converge, and PV gradients steepen, as resolution is increased. The PV-tongue-tip position, number of sub-vortices, zonal velocity profile and other quantitative measures are presented as specific modeling-accuracy results. SEAM produces solutions up to approximately T181 (approximately 70 km horizontal resolution) with 200 levels, much more efficiently than the Community-Climate-Model-2 dynamical core; but the latter verifies the lower-resolution (up to T85 on 48 levels) SEAM results.

INTRODUCTION

The stratospheric polar vortex is bounded by strong potential-vorticity gradients which isolate polar air from lower latitudes. A phenomenon of major atmospheric-research importance is the eventual mixing of these air masses, when the vortex is distorted by breaking planetary-scale Rossby waves.

This is the focus of the numerical simulation described here, as well as providing a test of “dynamical core” simulation (i.e., stripped of physical processes and parameterizations of a full general circulation model, other than those described by the primitive equations and below).

NUMERICAL METHOD

Initialization

Following Polvani and Saravanan [1], our initial model-state consists of a gradient-flow balanced axisymmetric-vortex: at time $t = 0$, as a function of latitude φ and pressure p , let the zonal wind $u = a\Omega u_i(\varphi, p)$, the meridional wind $v = 0$, the isobaric velocity $dp/dt \equiv \omega = 0$, the temperature $T = T_0 - R_d^{-1}a^2\Omega^2 \frac{\partial \Phi_i}{\partial \ln p}$ and the geopotential $\Phi = g_0 z_{\ln p} + a^2\Omega^2 \Phi_i(\varphi, p)$, where a , Ω and g_0 are the earth’s radius, angular frequency and gravity, $T_0 = 239.14\text{K}$ is the isotherm for a scale height of 7 km, R_d is the gas constant and $z_{\ln p}$ is log-pressure height. The nonlinear gradient-flow balance is

$$\frac{\partial \Phi_i}{\partial \varphi} = -u_i (2\mu + u_i \tan \varphi), \quad (1)$$

where $\mu \equiv \sin \varphi$, so the complete initial state only depends on u_i . We assign the vortex-edge latitude $\varphi_v = 60^\circ$ and impose $u_i(\varphi_z, p) = 0$ for $\varphi_z \equiv 37^\circ$ and all p . Moving equatorward from $\varphi = \pi/2$, we assume the initial absolute vorticity

$$\eta_i \equiv 2\mu - \frac{\partial u_i \cos \varphi}{\partial \mu} \quad (2)$$

is positive, almost constant until φ_v , where it decreases rapidly over a zone of width around $\Delta\varphi = 6^\circ$,

then again nearly constant until the “surf-zone” edge $\varphi_s \equiv 35^\circ$, followed by cubic decrease to zero at the equator, and solid-body rotation for $\varphi \leq 0$:

$$\eta_i(\varphi, p) \equiv \begin{cases} c_1 r'_h(\mu) + c_2, & \mu_s \leq \mu, \\ 2c_3\mu - 4c_4\mu^3, & 0 \leq \mu \leq \mu_s, \\ 2[1 + u_i(0, p)]\mu, & \mu \leq 0, \end{cases} \quad (3)$$

where the hyperbolic ramp function

$$r_h(\mu) \equiv \int_1^\mu r'_h(\mu') d\mu',$$

$$r'_h(\mu) \equiv 2^{-1} \left(1 + \tanh \frac{\mu - \mu_v}{\Delta\phi \cos \varphi_v} \right),$$

and the coefficients $c_n(p)$ must be determined as follows. From (2,3) follow

$$M(\mu, p) \equiv 1 - \mu^2 + u_i \cos \varphi = \int_\mu^1 \eta_i =$$

$$\begin{cases} -c_1 r_h(\mu) + c_2(1 - \mu), & \mu_s \leq \mu, \\ 1 + u_i(0, p) - c_3\mu^2 + c_4\mu^4, & 0 \leq \mu \leq \mu_s, \\ [1 + u_i(0, p)] \cos^2 \varphi, & \mu \leq 0. \end{cases} \quad (4)$$

Since $\varphi_v > \varphi_z > \varphi_s$ it follows immediately that

$$c_2(p) = \frac{r_h(\mu_z)M(\mu_v, p) - r_h(\mu_v)M(\mu_z, p)}{r_h(\mu_z)(1 - \mu_v) - r_h(\mu_v)(1 - \mu_z)},$$

$$c_1(p) = r_h(\mu_v)^{-1} [c_2(1 - \mu_v) - M(\mu_v, p)],$$

while ensuring continuity of (2,4) leads to

$$c_4(p) = \frac{M(0, p) - M(\mu_s, p)}{\mu_s^4} - \frac{c_1 r'_h(\mu_s) + c_2}{2\mu_s^3},$$

$$c_3(p) = 2^{-1} [c_1 r'_h(\mu_s) + c_2] \mu_s^{-1} + 2c_4 \mu_s^2.$$

It only remains to define $u_i(0, p) \equiv -20 \text{ m s}^{-1}$ and $u_i(\varphi_v, p) = [1 + D^{-1} z_{\text{in}p}] u_i(0, p)$, where D is the model height, for then (4) yields $u_i(\varphi, p)$, as shown in Fig. 1. The initial scaled-potential-vorticity (Π) profile is shown in Fig. 2. $\Pi \equiv \mathcal{P}T(\eta)/\mathcal{P}T_0(2\Omega)$, where $\mathcal{P}T(\eta) \equiv -g_0 \eta \frac{\partial}{\partial p} \theta(T)$ approximates the potential vorticity in isobaric coordinates and $\theta(T) \equiv T(10^5 \text{ Pa}/p)^{R_d/c_p}$ is the potential temperature.

Forcing

The model is forced by setting Φ at the surface for all time equal to $\Phi_a \cos \lambda (\sin \frac{9}{2} \phi)^2 (1 - e^{-t/\tau})$ for $40^\circ < \phi < 80^\circ$, and zero otherwise ($\lambda = \text{longitude}$), with decay time $\tau = 3 \text{ d}$ and amplitude $\Phi_a = 800 \text{ m}$. The forcing peaks at $\phi = 60^\circ = \varphi_v$, and increases monotonically in time. The effect is to instigate upward-propagating Rossby waves. Spurious reflection is prevented by a sponge layer near the model top, including Rayleigh damping of eddy velocity and Newton damping of T .

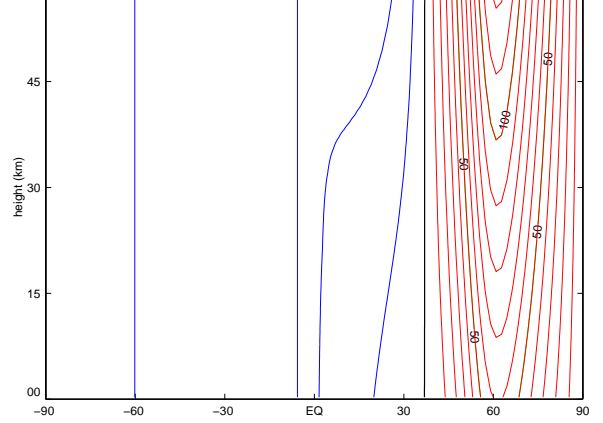


Figure 1: Initial zonal-wind isotachs (m s^{-1}) vs φ ($^\circ$, abscissa) and $z_{\text{in}p}$ (km, ordinate).

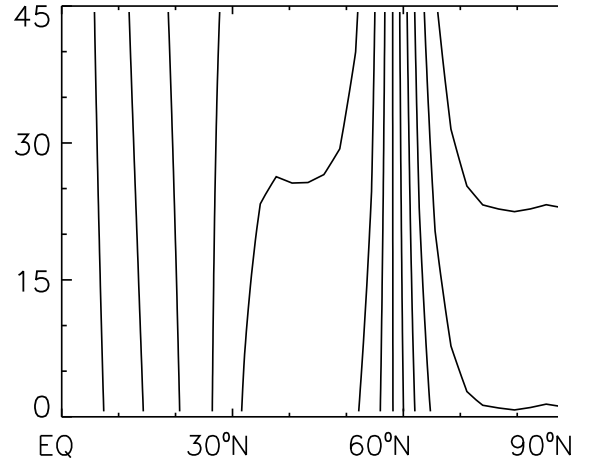


Figure 2: Isopleths of initial scaled potential vorticity, as in Fig. 1.

RESULTS

CCM2 Dynamical Core

The polar-vortex simulation was first carried out with the Community-Climate-Model-2 (CCM2) dynamical core with resolutions T42 and T85, on 48 levels. Since there is no analytical solution and higher-resolution CCM2 runs were expensive at the time, we verified all of the results presented here using a relatively new dynamical core, the *Spectral Element Atmospheric Model* [2–4]. The more efficient numerical algorithm made ≈ 180 runs on 200 levels easily doable. We computed 5.4×10^4 time steps on 2.2×10^7 collocation points in 2.5 days on 64 HP Exemplar processors. From the latter experiment, the Π isosurfaces in Figs. 3 and 4 indicate complex dynamical features: a primary Π “tongue,” succumbing to a secondary instability, leading to a

roll-up into a ring of five smaller sub-vortices. These features converge, and Π -gradients increase, as resolution increases.

Proposed modeling-accuracy test-case goals

The first quantity to reproduce in this simulation should be the profile of zonal-average zonal wind $\langle u \rangle_\lambda$ at φ_v , e.g., at day 20, as shown in Fig. 5.

A particular test of dynamical accuracy would be the isentropic Π -tongue-tip position $\tilde{r}(t, \theta)$. This may be quantified as the point of minimum radius-of-curvature of the $\Pi = 4/5$ contour. Fig. 3 shows this point's longitude change $\Delta\lambda_\Pi$ decreasing with time and altitude, independently. This corresponds to the long curves of constant $\Delta\lambda_\Pi$ which slope down relatively smoothly in Fig. 6, displaying a structure which should be reproduced. The more random-looking features in Fig. 6 are due to the numerous $\Pi = 4/5$ contours which proliferate at larger times and altitudes where the vortex is breaking up.

The area $A_\Pi(\theta, t)$ of the $\Pi = 4/5$ contours evolves with a qualitatively similar pattern, as shown in Fig. 7 for the low-resolution CCM2 simulation. This is a good measure of vortex erosion, as discussed in further detail in refs. 1, 5. However, it should be noted that higher-resolution simulation of the vortex filaments can lead to temporary vortex-area increase during the breakup, as in the SEAM simulation (not shown). We estimated $A_\Pi(\theta, t)$ by summing over points (λ, φ) with $\Pi(\lambda, \varphi, \theta, t) \geq 4/5$, weighted such that a constant field would give 4π sr.

Finally, it is important to obtain the correct number, five, of smaller vortices emerging from the break-up of the larger, initial vortex. The zonal-wavenumber-five character of the secondary instability is evident in the bottom panel of Fig. 4. To automatically extract the number of sub-vortices from the model data, we first removed all 2D wavenumbers above 12 (to eliminate very small vortices), then regridded the $\theta = 1.5 \times 10^3 \text{K}$ surface over the plane (to eliminate cutting of contours at $|\lambda| = \pi$) and automatically counted the number of $\Pi = 1$ contours. A typical contour evolution is shown in Fig. 8.

DISCUSSION

The existing dynamical-core test cases [6–8] are important, but mainly of a relatively low-order, statistical nature. We offer this polar-vortex simulation to fill the need for a complex yet predictable fore-

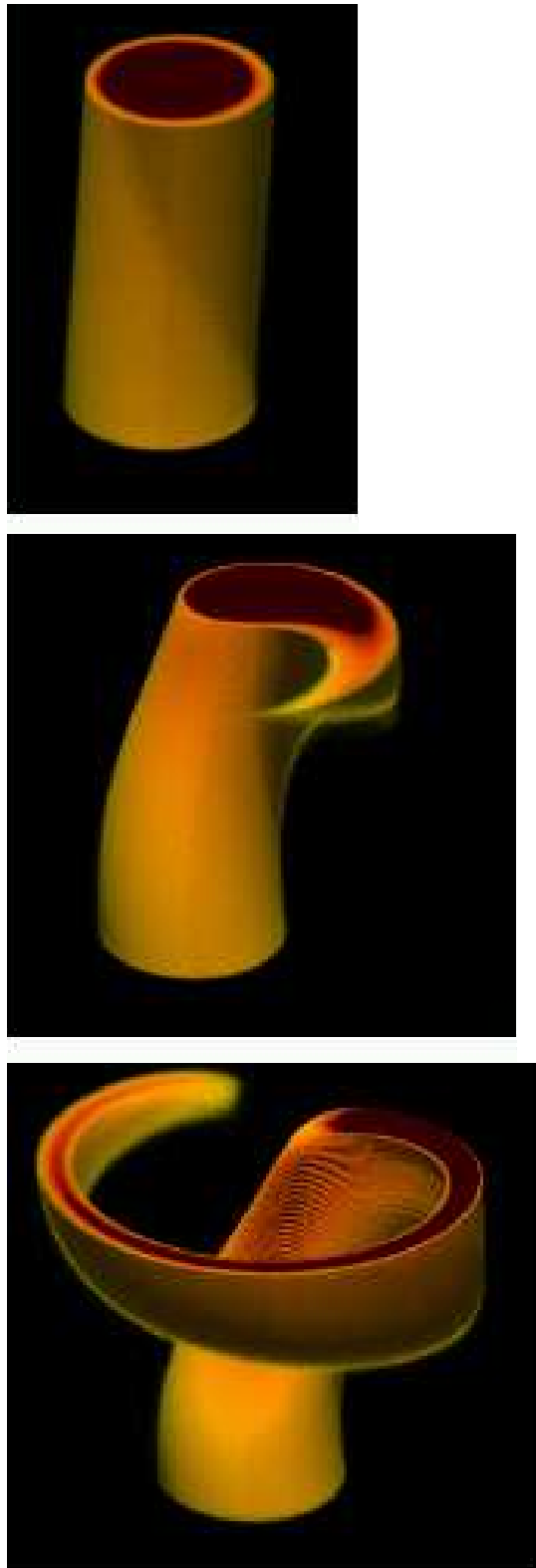


Figure 3: Isosurfaces of scaled potential vorticity, 3 snapshots, oblique view.

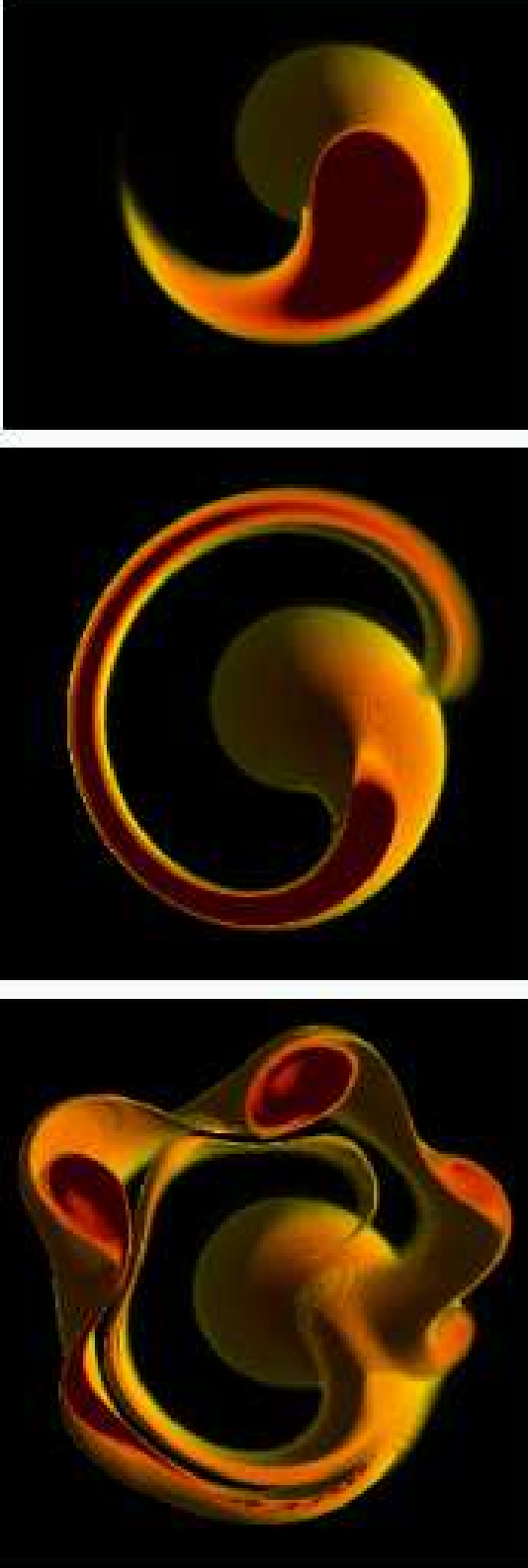


Figure 4: As in Fig. 3, view from above the North Pole, starting at second snapshot.

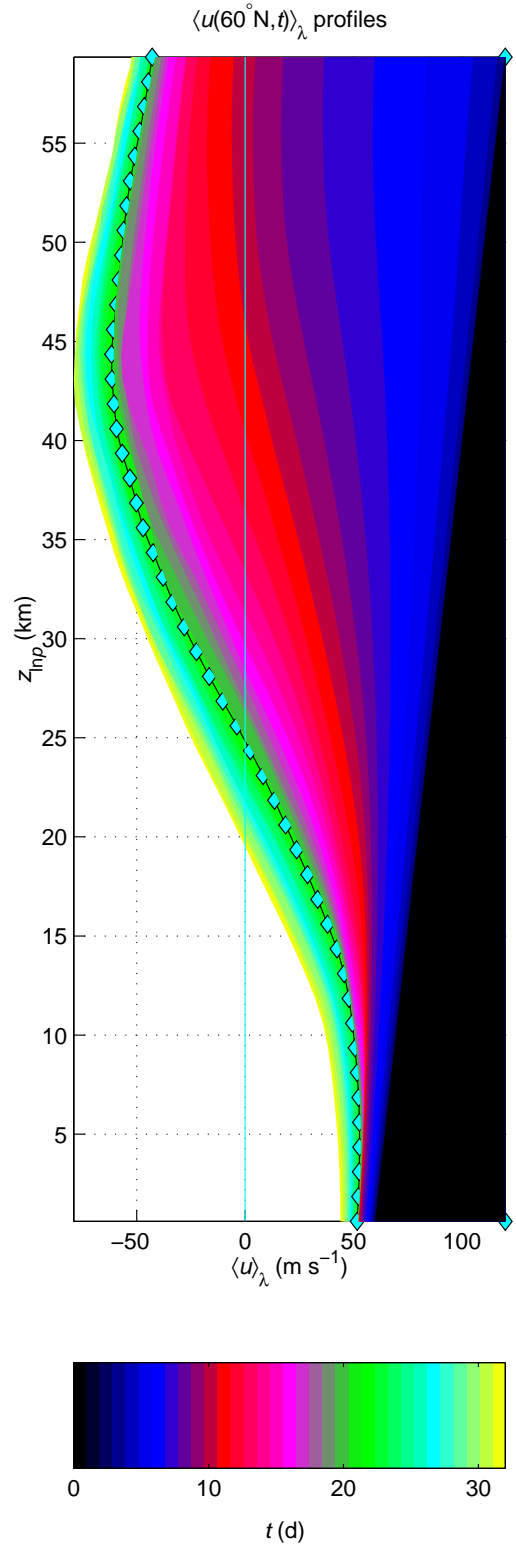


Figure 5: $\langle u \rangle_\lambda$ profiles (abscissa), as a function of t (d, color) and z_{inp} (km, ordinate). The diamond markers indicate $t = 20$ d.

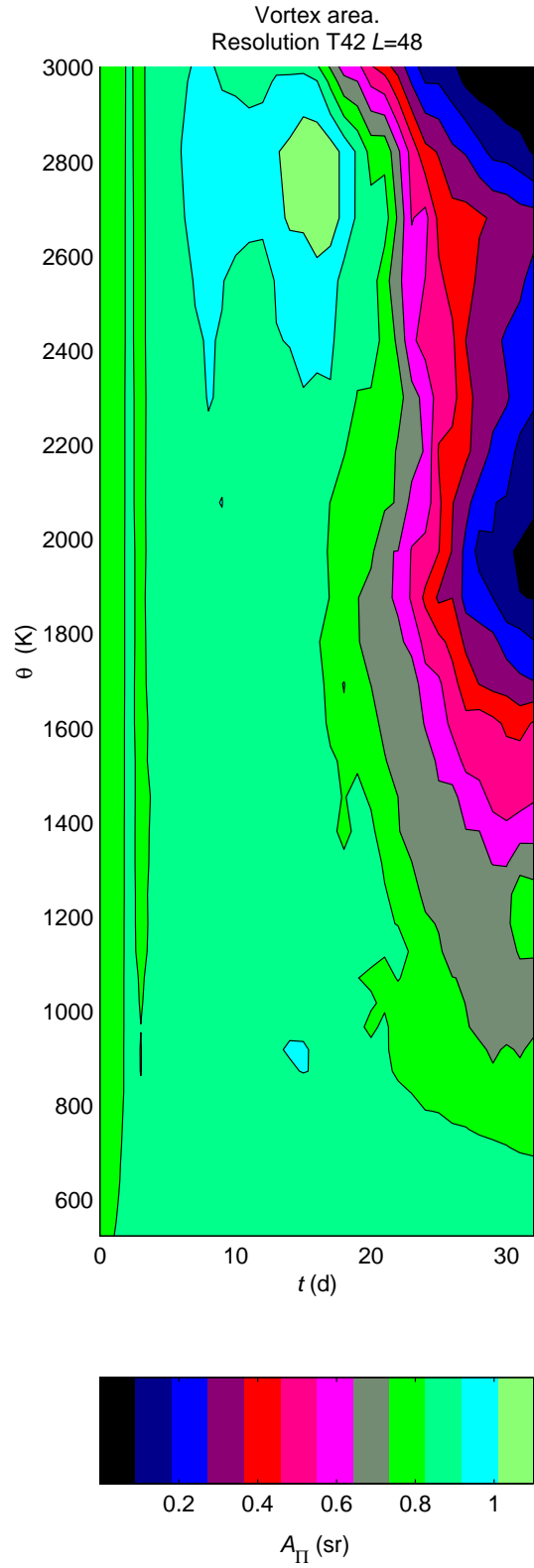
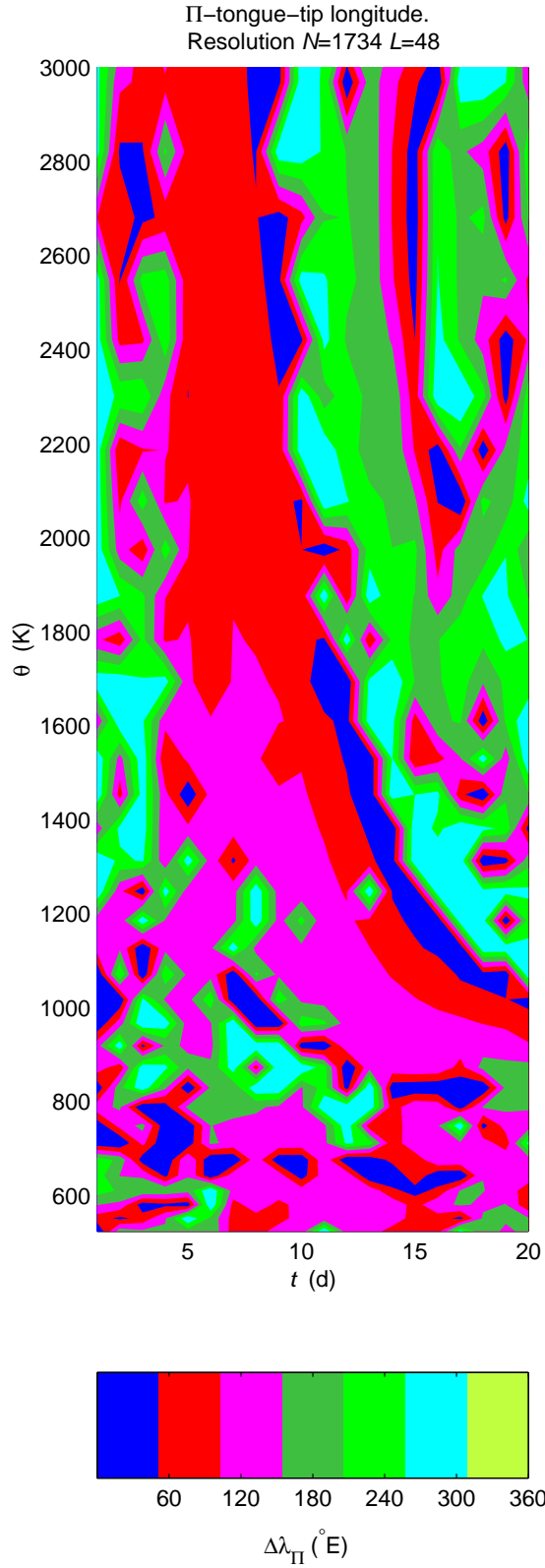


Figure 6: Isopleths of PV-tongue-tip longitude-change, $\Delta\lambda_{\Pi} \equiv \lambda_{\Pi}(\theta, t) - \lambda_{\Pi}(\theta, 1d)$ ($^{\circ}$, color), as a function of t (d, abscissa) and θ (K, ordinate).

Figure 7: Horizontal vortex-area $A_{\Pi}(\theta, t)$ (sr), as in Fig. 6.

Evolution of $\Pi=1$ contour on $\theta=1.5e+03K$,
Resolution $N=1734$ $L=200$

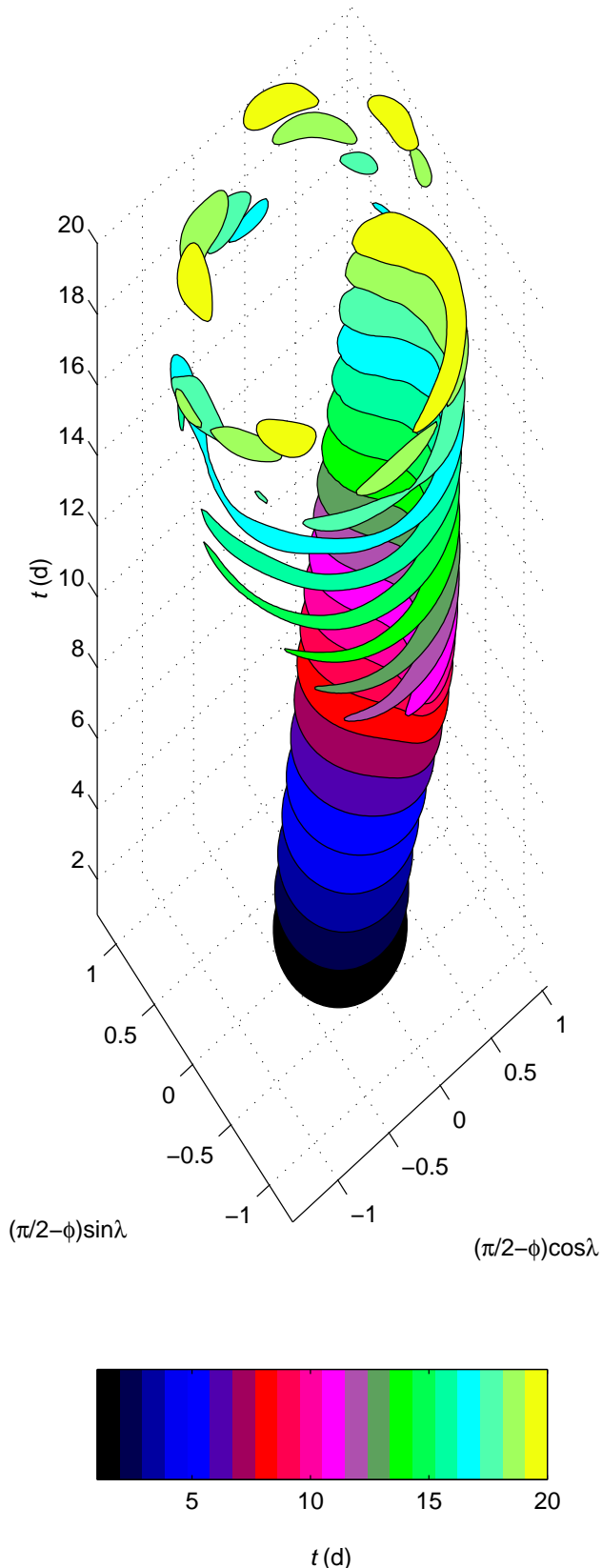


Figure 8: Evolution of the $\Pi = 1$ contour over the plane $(\pi/2 - \varphi)(\cos \lambda, \sin \lambda)$, as a function of t (d, vertical axis and color).

cast test case for 3D primitive equations. The diagnostics, namely, $\langle u \rangle_\lambda$, $\Delta \lambda_\Pi$, A_Π and the number of sub-vortices after breakdown, were essentially reproduced by the CCM2 dynamical core at T42 and T85, and by SEAM at $\approx T180$. See ref. 5 for details.

REFERENCES

- [1] L. M. Polvani and R. Saravanan. The three-dimensional structure of breaking rossby waves in the polar wintertime stratosphere. To appear in *J. Atmos Sci.*, and available on-line at http://www.columbia.edu/~lmp/lmp_pubs.html, 2000.
- [2] M. Taylor, J. Tribbia, and M. Iskandarani. The spectral element method for the shallow water equations on the sphere. *J. Comput. Phys.*, 130:92–108, 1997. Available on-line at http://www.scd.ucar.edu/css/staff/taylor/doe/spectral_elem.ps.gz.
- [3] M. Taylor, R. Loft, and J. Tribbia. Performance of a spectral element atmospheric model (SEAM) on the HP Exemplar SPP2000. Technical Report TN-439+EDD, NCAR, November 1997. Available on-line at <http://www.scd.ucar.edu/css/staff/taylor/doe/seam.ps.gz>.
- [4] A. Fournier, M. Taylor, and J. Tribbia. The spectral element atmospheric model: High-resolution parallel computation and response to regional forcing, 2000. In preparation.
- [5] A. Fournier, L. M. Polvani, R. Saravanan, and M. Taylor. The polar vortex as an initial-value test case for the spherical primitive equations, 2000. In preparation.
- [6] I. M. Held and M. J. Suarez. A proposal for the intercomparison of the dynamical cores of atmospheric general circulation models. *Bull. Amer. Meteor. Soc.*, 75:1825–1830, 1994.
- [7] D.L. Williamson, J.B. Drake, J.J. Hack, R. Jakob, and P.N. Swarztrauber. A standard test set for numerical approximations to the shallow water equations in spherical geometry. *J. Comput. Phys.*, 102:211–224, 1992.
- [8] G.J. Boer and B. Denis. Numerical convergence of the dynamics of a GCM. *Clim. Dyn.*, 13:359–374, 1997.